Progress In Electromagnetics Research, PIER 87, 105–115, 2008

PROPERTIES OF APPROXIMATE BESSEL BEAMS AT MILLIMETER WAVELENGTHS GENERATED BY FRACTAL CONICAL LENS

Y. Z. Yu and W. B. Dou †

State Key Lab of Millimeter Waves
Southeast University
Nanjing, Jiangsu 210096, China

Abstract—An axicon, which images a point source into a line along the optic axis, is used widely to generate an approximation to a Bessel beam. More recently many novel axicons, such as Fresnel axicons, Fractal axicons and fractal conical lenses (FCLs), have been proposed. Understanding the properties of Bessel beams generated by these axicons is very helpful to research their applications. However, in optical region, all of them are calculated approximately by the scalar theory. To accurately analyze FCLs when illuminated by a plane wave at millimeter wavelengths, the rigorous electromagnetic analysis method, which combines a two-dimension finite-difference time-domain (2-D FDTD) method and Stratton-Chu formulas, is adopted in our paper. By using this method, the properties of approximate Bessel beams generated by FCLs are analyzed and the conclusions are given.

1. INTRODUCTION

The term of Bessel beam, a family of non-diffracting beams, was introduced firstly by Durnin and co-workers in 1987 [1, 2]. A true Bessel beam is non-diffractive. This means that as it propagates, it does not diffract and spread out. It thus possesses many attractive properties, such as long depth of field and extremely narrow intensity profile. These properties together make Bessel beams extremely useful in many applications. In optics they could have potential applications, such as optical alignment, optical interconnection, and promotion of free electron laser gain [3], and they may be useful in measurement,

† The first author is also with School of Science, Quanzhou Normal University, Quanzhou, Fujian 362000, China

communications and imaging applications [4, 5] at mm- and sub mm-wavelengths. An ideal Bessel beam cannot be created, as it is unbounded and therefore requires an infinite amount of energy [6]. However, reasonably good approximations can be made. Currently, numerous approaches for generating Bessel beams have been proposed, such as axicons [4], computer-generated holograms (CGH's) [7, 8] and diffractive optical elements (DOE's) [9], among which the simplest and easiest realization scheme is using axicons. Accordingly, much interest has been provoked in design and analysis of axicons [10], and the number of axicon applications has also increased significantly in the last few years [11]. More recently many novel types of axicons, such as Fresnel axicons [12], Fractal axicons [13] and fractal conical lenses (FCLs) [14], have been proposed and investigated in optics. Moreover, these elements can also be used in quasi-optical or millimeter wave systems. Understanding the properties of Bessel beams generated by these axicons is very helpful to research their applications. However, all of these axicons are analyzed approximately by the scalar theory in optics. At our interesting bands, i.e., millimeter wave bands, it is known that the scalar-based analysis method is usually not suitable for calculating the electromagnetic fields diffracted by them. Therefore, the rigorous electromagnetic analysis method is necessary to analyze them accurately and credibly. We have already analyzed lots of lenses rigorously [15–19]. In this paper, we will analyze only FCLs when illuminated by a plane wave at millimeter wavelengths, owing to their unfamiliarities and novelties. Of course, other types of axicons can also be analyzed by the same way. However, the analysis method adopted in this paper is different from those presented in [15–19], that is, a two-dimension finite-difference time-domain (2-D FDTD) method in conjunction with Stratton-Chu formulas. The analysis results and conclusions are given in the end.

The present paper is organized as follows. The technique for generating FCLs is introduced in Section 2. Rigorous electromagnetic analysis method is described in Section 3. The numerical results and analyses are presented in Section 4. A brief summary is given in the last Section 5.

2. CANTOR-LIKE FRACTAL CONICAL LENSES (FCLS)

A fractal is generally a rough or fragmented geometric shape that can be split into parts, each of which is (at least approximately) a reduced-size copy of the whole [20], a property called self-similarity. A relatively simple example of such fractal is given by the Cantor set, which is introduced by German mathematician Georg Cantor in 1883

and defined as a set of points lying on a single line segment. The Cantor ternary set is the most common modern construction, and is created by repeatedly deleting the open middle thirds of a set of line segments, as shown in the upper part of Fig. 1(a). One starts by deleting the open middle third $(1/3, 2/3)$ from the interval $[0, 1]$, leaving two line segments: $[0, 1/3] \cup [2/3, 1]$. Next, the open middle third of each of these remaining segments is deleted, leaving four line segments: $[0, 1/9] \cup [2/9, 3/9] \cup [6/9, 7/9] \cup [8/9, 1]$. Continuing this process, at step S, there are 2^S segments of length 3^{-S} with $2^S - 1$ disjoint gaps located at the intervals $[p_{S,J}, q_{S,J}]$, with $J = 1, 2, \ldots, 2^S - 1$. For instance, at step $S = 2$, the Cantor ternary set has three gaps at $[1/9, 2/9]$, $[3/9, 6/9]$ and $[7/9, 8/9]$. In Fig. 1(a), only the first three steps of this process are illustrated for clarity.

The Cantor function, $F_S(x)$, based on the Cantor ternary set, is defined in the interval $[0, 1]$ as [14]

$$F_S(x) = \begin{cases} \dfrac{J}{2^S} & \text{if} \quad p_{S,J} \le x \le q_{S,J} \\ \dfrac{1}{2^S} \dfrac{x - q_{S,J}}{p_{S,J} - q_{S,J}} + \dfrac{J}{2^S} & \text{if} \quad q_{S,J} \le x \le p_{S,J+1} \end{cases}$$

with $J = 1, 2, \ldots, 2^S - 1$. The Cantor function $F_3(x)$ is illustrated in the lower part of Fig. 1(a).

A FCL is defined as a rotationally symmetric lens that is generated from the Cantor ternary set to a level of growth [13, 14]. The profile of FCL is matched to Cantor function $F_S(x)$ at a given step, S, as

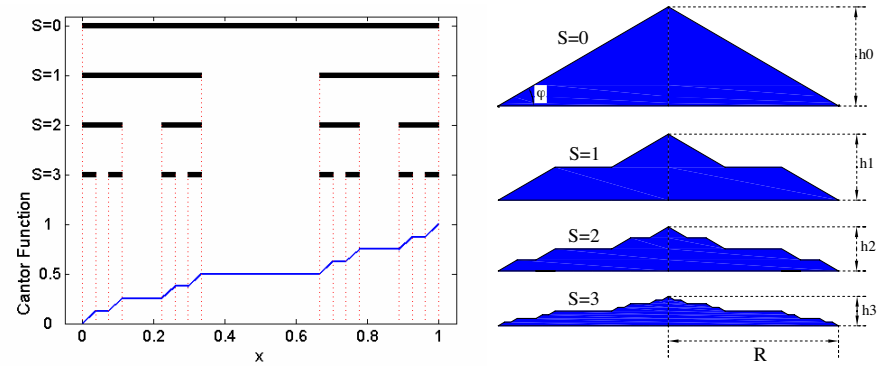

Figure 1. The upper part shows the Cantor ternary set for step $S = 0$, 1, 2, and 3, and the Cantor function $F_3(x)$ is illustrated in the lower part. (b) The profiles of FCLs at step $S = 0$, 1, 2, and 3, respectively.

shown in Fig. 1(b). Note that in order to keep a constant value of the open angles φ, at different steps S, the height of the FCL is $h_S = (2/3)^S h_0$, where h_0 is the height of a FCL at $S = 0$ corresponding to the conventional conical lens (CL).

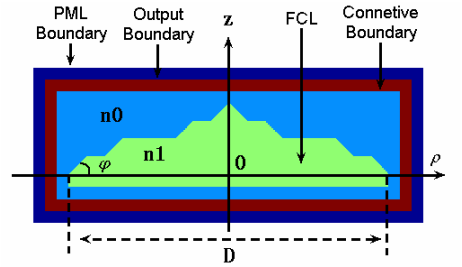

Figure 2. Schematic diagram of 2-D FDTD computational model.

3. RIGOROUS ELECTROMAGNETIC ANALYSIS METHOD

The FDTD method [21] has been demonstrated as a powerful and efficient technique for calculating the electromagnetic behavior of a structure throughout decades [22, 23]. So, it has been used extensively in many areas of electromagnetics [24–28]. Because of rotational symmetry of a FCL, thus, the 2-D FDTD method can be employed to compute the electromagnetic fields diffracted by the FCL in the near region. The computational model of the 2-D FDTD method is shown schematically in Fig. 2, in which the FCL, with the open angle φ and aperture diameter D, is totally embedded into the FDTD grid and used to convert an incident plane wave into an approximate Bessel beam. To excite the entire FDTD grid, a total-scattered field approach is applied to introduce a normally incident plane wave. The computational region of the 2-D FDTD method is truncated by using PML [29] absorbing boundary conditions (ABCs) in the near region, owing to the limitation of computational time and memory. Because of its excellent absorbing characteristic, the thickness of the PML is only a few meshes, which can greatly save the required memory and decrease computational time. Therefore, in order to accurately evaluate electromagnetic fields in the far region, Stratton-Chu integral formulas are applied and given by [30]

$$\vec{E}(\vec{r}) = \int_L \left\{ j\omega\mu \left[\vec{n} \times \vec{H}(\vec{r}') \right] G_0(\vec{r}, \vec{r}') - \left[\vec{n} \times \vec{E}(\vec{r}') \right] \times \nabla' G_0(\vec{r}, \vec{r}') - \left[\vec{n} \cdot \vec{E}(\vec{r}') \right] \nabla' G_0(\vec{r}, \vec{r}') \right\} dL'$$

$$\vec{H}(\vec{r}) = -\int_L \left\{ j\omega\varepsilon \left[\vec{n}\times\vec{E}(\vec{r}')\right] G_0(\vec{r},\vec{r}') + \left[\vec{n}\times\vec{H}(\vec{r}')\right]\times\nabla' G_0(\vec{r},\vec{r}') + \left[\vec{n}\cdot\vec{H}(\vec{r}')\right]\nabla' G_0(\vec{r},\vec{r}') \right\} dL' \quad (1)$$

where $\vec{r} = (\rho, z)$ and $\vec{r}' = (\rho', z')$ denote an arbitrary observation point in the far region and an source point on the output boundary of the 2-D FDTD model, respectively; unit vector $\vec{n}$ is the outer normal of the closed curve, L, of the output boundary; $G_0(\vec{r},\vec{r}') = -\frac{i}{4}H_0^{(2)}(k|\vec{r}-\vec{r}'|)$, is the 2-D scalar Green's function in free space and k is the wave number; ω is the angular frequency; ε and μ are the permittivity and permeability, respectively.

First, the fields, $\vec{E}(\vec{r}')$ and $\vec{H}(\vec{r}')$, on the output boundary are obtained by 2D-FDTD method. Then, these fields can be considered as secondary sources and substituted into Eq. (1) to obtain fields, $\vec{E}(\vec{r})$ and $\vec{H}(\vec{r})$, at arbitrary observation point in the far region. Note that the integral herein is over the closed curve, L, of the output boundary.

4. NUMERICAL RESULTS AND ANALYSES

4.1. The Properties of Bessel Beams Generated by FCLs at Different Steps

To investigate the properties of Bessel beams generated by FCLs at different steps when illuminated by a plane wave of unit amplitude, Fig. 3 displays the axial intensity distributions and corresponding transverse patterns at $z_{\max}$ planes for step $S=0$, 1, 2 and 3, respectively. Note that on the left side of Fig. 3, as well as in Fig. 4 and Fig. 5, the z-axis is marked using logarithmic graduation for clarity in the near region. The parameters used in Fig. 3 are as follows: an incident wavelength is $\lambda = 3\,\text{mm}$, the open angle is $\varphi = 10°$, and the diameter is $D = 24\lambda$, the refractive indexes of the axicon and the air are $n_1 = 1.4491$ (Teflon) and $n_0 = 1.0$, respectively. From the left side of Fig. 3, we can see apparently that the oscillation amplitudes of all these curves increase slowly, and reach their respective maximum value then decrease sharply, as the propagation distance z increases. The maximum values of on-axis intensities in Fig. 3(a), Fig. 3(c), Fig. 3(e) and Fig. 3(g) are 6.6172, 3.4386, 6.4523 and 7.6588, respectively; and they are located at $z = 60.14\lambda$, 150.75λ, 165.53λ and 175.86λ, respectively. Therefore, the larger the step S is, the farther is the propagation distance z. Moreover, the larger the step S is, the higher is the average value of axial intensity, except the step $S=0$ in which it reaches the maximum. This is interpreted as the increasing

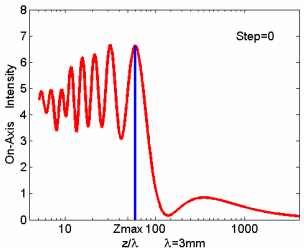

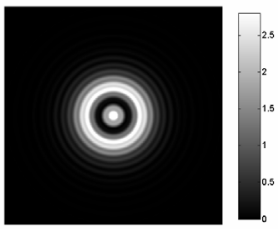

(a) the maximum axial intensity is 6.6172 located at z=60.14λ. (b)

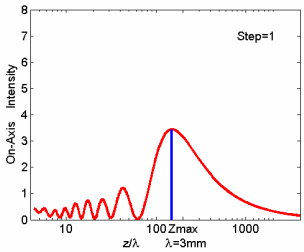

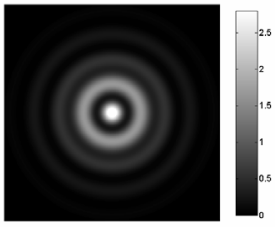

(c) the maximum axial intensity is 3.4386 located at z=150.75λ. (d)

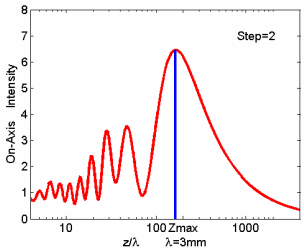

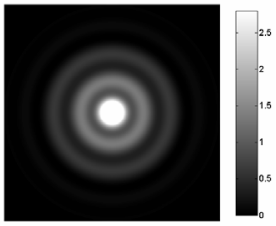

(e) the maximum axial intensity is 6.4523 located at z=165.53λ. (f)

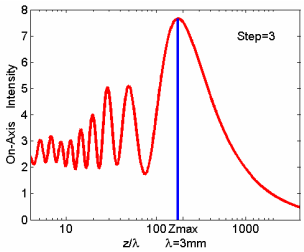

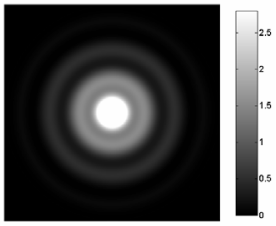

(g) the maximum axial intensity is 7.6588 located at z=175.86λ. (h)

Figure 3. The axial intensity distributions and transverse patterns for step $S = 0$, 1, 2, and 3, respectively. The axial intensity distributions are illustrated on the left side and corresponding transverse patterns at $z_{\max}$ planes are shown on the right side. Note that on the left side the z-axis is marked using logarithmic graduation for clarity in the near region.

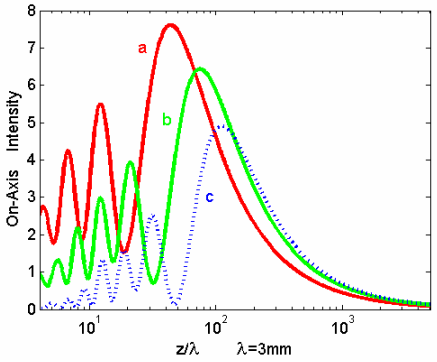

Figure 4. The influence of aperture diameters D on axial intensities, curves a, b and c corresponding to $D = 12, 16, 20\lambda$, respectively. The maximum intensities of curves a, b and c are 7.6133, 6.4328, 4.9013, respectively, and their locations at z-axis are 43.64λ, 74.64λ, 110.86λ, respectively.

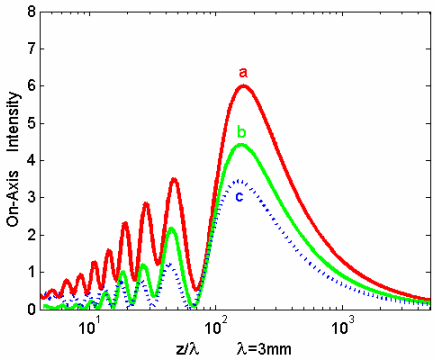

Figure 5. The influence of open angles φ on axial intensities, curves a, b and c corresponding to $\varphi = 7, 9, 10^\circ$, respectively. The maximum values of curves a, b and c are 5.9949, 4.4189 and 3.4386, respectively, whose locations at z-axis are 164.92λ, 158.08λ and 150.75λ, respectively.

convergence while the step S increase, but except the step $S = 0$ in which the FCL has the largest convergence performance and therefore has the highest average value of axial intensity. It is also found that the farther the propagation distance z is, the lower is the oscillation frequency.

In order to study the properties of the transverse patterns, we typically present them only at $z_{\max}$ planes on the right side of Fig. 3.

Side bars illustrate the relative magnitudes. It is indicated that all of FCLs illuminated by a plane wave can generate Bessel beams which are only the approximations to the ideal. In addition, it can be seen clearly that the larger the step S is, the larger the diameter of central spot becomes.

4.2. The Influence of Aperture Diameters D on Axial Intensities

To further research the characteristics of FCLs, in this Subsection 4.2 and next Subsection 4.3, the studies of the properties of Bessel beams produced by FCLs with different aperture diameters and open angles are made respectively. The influence of aperture diameters D on axial intensities are investigated under the conditions of step $S = 1$ and the open angle $\varphi = 10°$. The axial intensities along the z-axis are displayed in Fig. 4, when the FCLs, with $D = 12$, 16, 20λ, respectively, are illuminated by a plane wave of unit amplitude. The curves a, b and c in Fig. 4 correspond to the aperture diameters $D = 12, 16, 20\lambda$, respectively. The maximum intensities of curves a, b and c are 7.6133, 6.4328, 4.9013, respectively, and their locations at z-axis are 43.64λ, 74.64λ, 110.86λ, respectively. Thus, under the conditions of fixed step S and open angle φ, a conclusion, that the larger the aperture diameter is, the farther is the propagation distance z, and the smaller is the oscillation amplitude, can be easily reached from Fig. 4.

4.3. The Influence of Open Angles φ on Axial Intensities

Assuming that step $S = 1$ and $D = 24\lambda$, we examine the influence of open angles φ on axial intensities. When the FCLs, with $\varphi = 7, 9, 10°$, respectively, are illuminated by a plane wave of unit amplitude, the axial intensities of them are illustrated in Fig. 5, where the curves a, b and c correspond to the open angles $\varphi = 7, 9, 10°$, respectively. The change tendencies of three curves in Fig. 5 are similar to those in Fig. 4. The maximum values of curves a, b and c are 5.9949, 4.4189 and 3.4386, respectively, whose locations at z-axis are 164.92λ, 158.08λ and 150.75λ, respectively. Therefore, a conclusion can be easily draw from Fig. 5 that when the step S and diameter D of FCLs is fixed, the smaller the open angle φ is, the farther is the propagation distance z, and the larger is the oscillation amplitude.

5. SUMMARY

The rigorous electromagnetic analysis method, which combines a 2-D FDTD method and Stratton-Chu formulas, has been employed to accurately analyze the FCLs illuminated by a plane wave. Results show that not only the axial but also the transverse intensity distributions depend on the step S of growth. The different step S corresponds to different convergence performance, and therefore there are different axial and transverse intensity distributions. In addition, at a fixed step S, the on-axis intensity distributions are depended on the diameter and open angle of the FCLs. These results give us an indication that the desired Bessel beam at millimeter wavelengths can be acquired by selecting the diameter and open angle of a FCL with suitable step S.

ACKNOWLEDGMENT

This work is supported by NSFC under grant 60621002, and the Natural Science Foundation of Fujian Province of China (No. A0610027).

REFERENCES

1. Durnin, J., "Exact solutions for nondiffracting beams. I. The scalar theory," *J. Opt. Soc. Am. A*, Vol. 4, No. 4, 651–654, 1987.
2. Durnin, J., J. J. Miceli, Jr., and J. H. Eberly, "Diffraction-free beams," *Phys. Rev. Lett.*, Vol. 58, No. 15, 1499–1501, 1987.
3. Li, D., K. Imasaki, S. Miyamoto, S. Amano, and T. Mochizuki, "Conceptual design of Bessel beam cavity for free-electron laser," *Int. J. Infrared Millim. Waves*, Vol. 27, No. 4, 165–171, 2006.
4. Monk, S., J. Arlt, D. A. Robertson, J. Courtial, and M. J. Padgett, "The generation of Bessel beams at millimetre-wave frequencies by use of an axicon," *Opt. Commun.*, Vol. 170, 213–215, 1999.
5. Mahon, R. J., W. Lanigan, J. A. Murphy, N. Trappe, S. Withington, and W. Jellema, "Novel techniques for millimeter wave imaging systems operating at 100 GHz," *Proc. SPIE Int. Soc. Opt. Eng.*, Vol. 5789, 93–100, 2005.
6. Garcés-Chávez, V., D. McGloin, H. Melville, W. Sibbett, and K. Dholakia, "Simultaneous micromanipulation in multiple planes using a self-reconstructing light beam," *Nature*, Vol. 419, No. 6903, 145–147, 2002.
7. Salo, J., J. Meltaus, E. Noponen, et al., "Millimeter-wave Bessel

beams using computer holograms," *Electron. Lett.*, Vol. 37, No. 13, 834–835, 2001.

8. Meltaus, J., J. Salo, E. Noponen, et al., "Millimeter-wave beam shaping using holograms," *IEEE Trans. Microwave Theor. Tech.*, Vol. 51, No. 4, 1274–1279, 2003.
9. Yu, Y. Z. and W. B. Dou, "Generation of Bessel beams at mm- and sub mm-wavelengths by binary optical elements," *Int. J. Infrared Millim. Waves*, Vol. 29, No. 7, 693–703, 2008.
10. Pu, J. X. and S. J. Nemoto, "Design and analysis of diffractive axicons for Gaussian beam illumination," *Chin. J. Lasers B*, Vol. 10, No. 3, 228–232, 2001.
11. Jaroszewicz, Z., A. Burvall, and A. T. Friberg, "Axicon-the most important optical element," *Opt. Photonics News (USA)*, Vol. 16, No. 4, 35–39, 2005.
12. Golub, I., "Fresnel axicon," *Opt. Lett.*, Vol. 31, No. 12, 1890–1892, 2006.
13. Monsoriu, J. A., C. J. Zapata-Rodriguez, and W. D. Furlan, "Fractal axicons," *Opt. Commun.*, Vol. 263, No. 1, 1–5, 2006.
14. Monsoriu, J. A., W. D. Furlan, P. Andres, and J. Lancis, "Fractal conical lenses," *Opt. Express*, Vol. 14, No. 20, 9077–9082, 2006.
15. Yin, H. P. and W. B. Dou, "Analysis of an extended hemispherical lens antenna at millimeter wavelengths," *Journal of Electromagnetic Waves and Applications*, Vol. 16, No. 9, 1209–1222, 2002.
16. An, G. and W. B. Dou, "Analysis of a sphere lens quasi-optical monopulse antenna/feed structure," *Journal of Electromagnetic Waves and Applications*, Vol. 19, No. 1, 83–93, 2005.
17. Dou, W. B. and Z. L. Mei, "Electromagnetic analysis of symmetrical diffractive lens with small F-number and electrical large size," *Journal of Electromagnetic Waves and Applications*, Vol. 19, No. 10, 1359–1374, 2005.
18. Wang, Z. X. and W. B. Dou, "Design and analysis of several kinds of dielectric lens antennas," *Journal of Electromagnetic Waves and Applications*, Vol. 20, No. 12, 1643–1653, 2006.
19. Wang, Z. X. and W. B. Dou, "Design and analysis of thin diffractive/refractive lens antennas," *Journal of Electromagnetic Waves and Applications*, Vol. 20, No. 15, 2239–2251, 2006.
20. Mandelbrot, B. B., *The Fractal Geometry of Nature*, W. H. Freeman, New York, 1983.
21. Yee, K. S., "Numerical solution of initial boundary value problems involving Maxwell equations in isotropic media," *IEEE Trans.*

Antennas Propag., Vol. 14, No. 3, 302–307, 1966.

22. Zhang, X., J. Fang, K. K. Mei, and Y. W. Liu, "Calculations of the dispersive characteristics of microstrips by the time-domain finite difference method," *IEEE Trans. Microwave Theor. Tech.*, Vol. 36, No. 2, 263–267, 1988.
23. Sheen, D. M., S. M. Ali, M. D. Abouzahra, and J. A. Kong, "Application of the three-dimensional finite-difference time-domain method to the analysis of planar microstrip circuits," *IEEE Trans. Microwave Theor. Tech.*, Vol. 38, No. 7, 849–857, 1990.
24. Ji, F., E. K. N. Yung, R. S. Chen, et al., "FDTD analysis of Y-junction microstrip circulator with a ferrite sphere," *Journal of Electromagnetic Waves and Applications*, Vol. 17, No. 11, 1631–1641, 2003.
25. Golestani-Rad, L., J. Rashed-Mohassel, and M. M. Danaie, "Rigorous analysis of EM-wave penetration into a typical room using FDTD method: The transfer function concept," *Journal of Electromagnetic Waves and Applications*, Vol. 20, No. 7, 913–926, 2006.
26. Ali, M. and S. Sanyal, "FDTD analysis of dipole antenna as EMI sensor," *Progress In Electromagnetics Research*, PIER 69, 341–359, 2007.
27. Afrooz, K., A. Abdipour, A. Tavakoli, et al., "Time domain analysis of active transmission line using FDTD technique (application to microwave/mm-wave transistors)," *Progress In Electromagnetics Research*, PIER 77, 309–328, 2007.
28. Ali, M. and S. Sanyal, "A numerical investigation of finite ground planes and reflector effects on monopole antenna factor using FDTD technique," *Journal of Electromagnetic Waves and Applications*, Vol. 21, No. 10, 1379–1392, 2007.
29. Berenger, J. P., "A perfectly matched layer for the absorption of electromagnetic waves," *J. Comput. Phys.*, Vol. 114, No. 2, 185–200, 1994.
30. Stratton, J. A., *Electromagnetic Theory*, McGraw-Hill, New York, 1941.